Joint Optimal PMU Placement and Data Pruning for Resource Efficient Smart Grid Monitoring

Akash Kumar Mandal and Swades De

***Abstract*—This paper proposes a novel joint system-aware data pruning and optimal phasor measurement unit (PMU) placement framework for smart grid monitoring. Mathematical modeling of the spatial error propagation across the system due to distorted reconstruction of direct measurements at the phasor data concentrator is undertaken. The node-level data pruning is analyzed on a large-scale data from the PMUs on IEEE 6, 14, 30, and 57-bus system infrastructure, under conventional deployment statistics. The analysis is extended for system-level data traffic reduction, and a revised optimal PMU placement is proposed. It is observed that the joint optimal PMU placement and system-aware optimal data pruning is able to achieve up to 95% bandwidth saving per PMU data communication. With the revised optimal PMU placement, the overall system-level communication resource consumption is reduced by $\geq 32\%$, while ensuring a predefined monitoring error threshold across the grid.**

***Index Terms*—Optimal PMU placement, resource efficiency, smart PMU communication, spatial error propagation, system-aware data pruning**

I. Introduction

The inclusion of renewables along with conventional sources has resulted in uncertainty in generation, transmission, and distribution process, leading to wideband disturbance propagation in modern grids [1]. This has motivated the power industry to include communication in the conventional smart grid monitoring setup [2]. Furthermore, rapid growth in power demands and the idea of decentralized generation requires stringent grid monitoring [3]. Phasor measurement units (PMUs) serve this purpose with highly accurate and time-stamped values of important system health variables [4], [5]. PMU placement strategies proposed in literature are solely based on attaining grid observability, while they ignore the smart communication aspect. High dimensionality of the PMU dataset makes the data processing difficult at the phasor data concentrators (PDCs) [6]. Lesser possibility of interaction between PMU datasets at the PDCs makes the grid monitoring inter-area disjoint. This has motivated the utilities to employ appropriate data pruning techniques. In such arrangements, quantification of reconstruction error is crucial in accurate state estimation and stability analysis of power system.

Moreover, defining grid stability based on electro-mechanical disturbances is insufficient in modern grids; rather understanding the electromagnetic spectra from such disturbances is crucial. The idea of wideband impedance has redefined the notion of disturbance, leading to a wideband study of steady-state or quasi-steady-state [7]. This aspect of wideband disturbance propagation makes real-time data communication from fast PMUs further pertinent. However, high sampling rate in such real-time systems generates huge data, which is difficult to communicate and analyze in real-time. Moreover, high cost of these devices call for an optimal placement policy, specially in systems with high node cardinality. While several node-level data pruning algorithms are proposed for PMU-to-PDC communication, they do not study the system-level impact. Low latency tolerance of these time-critical systems make these errors detrimental in system health monitoring. Further, the impulsive noise from power lines introduces large errors in the transmission of such data through smart grid wireless channels [8]. Thus, an efficient PMU-to-PDC communication requires a jointly optimal PMU deployment and system-aware data pruning. Also, for effective real-time data pruning in dynamic systems, it is important to model the evolution of error through its pseudo-monitored parts, which motivates the need to revisit the PMU placement optimization.

The authors are with the Department of Electrical Engineering and Bharti School of Telecommunication and Management, IIT Delhi, New Delhi 110016, India.

A. Literature Review and Motivation

The work in literature is broadly put in to three sets. The first set [9], [10] proposed node-level data pruning for smart PMU-to-PDC communication. The work in [11], [12] focused on the non-real time compression strategies, while [13] addressed its real-time counterpart for smart grid monitoring. The approach in [14] used principal component analysis (PCA) for node-level data compression at the smart meter, with [15] adding a discrete-cosine transform-based second stage to the PCA phase. The work in [16], [17] employed machine learning techniques at PDC in approximating the data collected at the PMU, thereby reducing the bandwidth consumption. Though these approaches considered node-level data pruning in real, semi-real, or non-real time smart grid communication, *they did not capture the system level impact of the reconstruction error. Thus, there is a need to fill this gap by considering system-aware PMU data pruning in smart grid networks.* Further, event-driven PMU-to-PDC communication for bandwidth saving severely undermines the capabilities of PMU data for preemptive event forecasting and load modeling using critical system parameters monitored by the PMU. Also, it heavily impairs the real-time feature of the data and increases the odds of data-based attacks [18]. Consequently, the industry prefers a more real-time approach instead of event-driven PMU-to-PDC communication even in a hierarchical power system communication infrastructure [19], [20].

The second set [21], [22], [23] studied the optimal PMU placement for different power system topologies from observability viewpoint. The work in [24] used deterministic

optimization tools, while [25], [26] used machine learning techniques to find the optimal solution. The work in [27], [28] revisited the optimal PMU placement problem under different kinds of fault scenarios. Further, [29] and [30] considered various contingencies and measurement redundancies in formulating the PMU placement optimization problem. A subset of these formulations extended the analyses to estimate parameters for the remaining nodes, called as pseudo-monitored nodes. The studies in [31], [32] used direct measurements noted by the PMUs in a conventional optimal deployment scenario for estimating the attribute values at the pseudo-monitored nodes. The work in [33] used the direct PMU data to estimate the transmission line parameters, while [34] used modes and mode shapes to estimate the system parameters. Though these works characterized grid observability using PMU data, they did not address the communication aspect. Thus, resource overloading in a full-fledged PMU-to-PDC communication enabled smart grid remains unexplored. To this end, *the prospect of PMU data pruning and the effect of error introduced data reconstruction needs to be investigated, which also motivates to revisit the optimal PMU placement problem.*

The final set [35], [36] deal with efficient pseudo-measurement bounds to achieve numerical observability. The approach in [37] proposed a weighted least square error minimization for guaranteeing efficient state estimation using PMU measurements. The study in [38] added a post processing step as a linear problem before using the values in power system state estimation. It highlights the possibility of measurement error in the PMUs. *Though most of the works discussed the effects of erroneous measurements on impairing the estimated pseudo-measurements, PMU placement and measurement error propagation dependent system-level performance were not investigated. As noted in [39], accounting for PMU measurement limitations and associated optimum PMU deployment will be more critical in future heterogeneous smart grids.*

To sum up, the existing works, while optimizing the power system aspects, do not address joint PMU placement and data pruning for network resource efficiency. We argue that, accounting for the communication aspects while optimizing the PMU deployment will enhance the resource efficiency without compromising on the system observability. An individual node-level PMU data pruning was studied in [40]. As an advance, this work considers joint optimal PMU data pruning and network-wide PMU deployment by accounting for the system-level impact, where the practical constraint of limited number of current monitoring channels in a PMU is also considered. The system state awareness is achieved by modeling spatial error propagation (SEP) and node sensitivity. As a consequence, the overall strategy maximizes communication resource efficiency in smart grid health monitoring.

B. Contributions and Significance

This paper proposes a novel jointly optimal PMU placement and system-aware data pruning framework for smart PMU-to-PDC communication. Optimum PMU placement problem is re-formulated from the smart grid communication perspective. The key contributions of this work are as follows:

1) A system-aware data pruning framework for PMU-to-PDC data communication is proposed and mathematical modeling of SEP in the pseudo-monitored node estimates is presented. For this purpose, most sensitive node and most sensitive parameter are defined.
2) An optimum PMU placement problem based on weighted grid incidence matrix, that also minimizes the data communication bandwidth consumption, is formulated based on system-aware data pruning.
3) SEP on current, voltage, active and reactive power estimates are studied in detail for an IEEE 6-bus system.
4) The performances of optimum PMU placement with node-level data pruning, and joint optimal PMU placement and system-aware data pruning are analyzed for various IEEE test systems as well as real power networks.
5) System observability and resource utilization performances of the proposed framework are quantified under different grid conditions (PMU failure and line outage).

Simulation results demonstrate that, PMU placement based on observability alone is insufficient in achieving optimum utilization of communication resources. The added redundancy by the virtue of joint optimal PMU placement and data pruning reduces the communication bandwidth consumption by $\geq 32\%$ while keeping the estimation error within a tolerable limit. Thus, the proposed strategy in this paper offers additional benefit of network resource saving in grid health data communication. Further, joint optimal placement adds robustness to grid adversities, such as PMU failure and line outage.

Section II defines the system model. Section III presents the joint optimal PMU placement and data pruning formulation. Section IV presents the analysis on IEEE 6-bus system, with results and conclusion in Sections V and VI, respectively.

II. System Model

Fig. 1 shows the system model used in proposing the joint optimal PMU placement and system-aware data pruning in smart grid. Real-time health monitoring and state estimation using PMUs is considered. These PMUs generate data at a high rate and transmit to the PDCs over smart grid channels. PMU installed at node i has c_i current channels, with node order o_i, s.t. $c_i \leq o_i$. The 'node order' o_i represents the number of nodes directly connected to the node i. The raw data generated by the PMUs is pruned to save the communication bandwidth. The PDCs work in sync with these PMUs to receive the pruned data and reconstruct the original data. We consider an S-bus system with PMUs directly monitoring W buses, s.t. $W \leq S$. Note that since the PMUs are optimally placed, not all nodes have a dedicated PMU.

In this work, we consider only current and voltage phasor estimations using the measured parameters in the modeling, thus studying the spatial error propagation (SEP). We consider a scenario with smart data transmission, with all these PMUs communicating among themselves and also with the central PDC. The PDCs estimate the critical power system parameters ensuring complete grid characterization. Further, since smart data transmission reduces the data redundancy, it leads to distortion during reconstruction of the pruned data at the

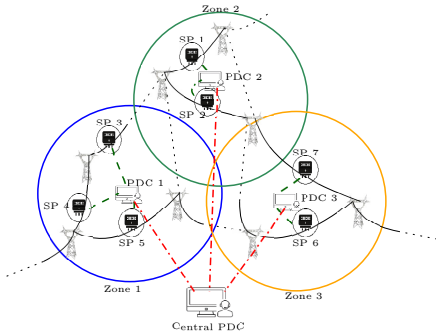

Fig. 1: System model for smart PMU (SP) communication.

PDC. Therefore, $\tilde{x}^t_{i,D_j} = x^t_{i,D_j} + \Delta x^t_{i,D_j}$, where $\tilde{x}^t_{i,D_j}$ is the reconstructed value against the true value of the ith data attribute at time t given by x^t_{i,D_j}, and $\Delta x^t_{i,D_j}$ is the error.

Remark 1. *The proposed data pruning is implemented on a PMU mounted on the incomer bay of a* 11 *kV*/440 *V,* 50 *Hz substation, reporting data over a wireless channel using WiFi to a PDC within a radius of* 1 *km. Data pruning algorithm at the PMU run on a Broadcom BCM*2837 64*-bit quad core processor, while the PDC operates on an E*3-1285 *v*6 *CPU.*

Note that, while this study considers a system-level optimization by accounting for the inter-PMU data dependence, proposing or studying communication among PMUs from multiple jurisdictions is not in its scope. To summarize, the research work presented in this manuscript suggests an improved way of utilizing the available communication network resources in a hierarchical communication setup, while simultaneously ensuring that the optimal PMU deployment along with the data pruning framework provides sufficient grid observability.

III. Joint Optimal PMU Placement and System-Aware Data Pruning

Let the PMU installed at bus i has sufficient current channels. Then, the probability that $L_{i,j}$ is monitored, given k_m out of remaining $o_i - 1$ incident lines are already monitored, is $Pr(\mathscr{Z}) = Pr[L_{i,j} = 1 | \prod_{j\in\{1,\cdots,k_m\}|k_m\leq o_i} L_{i,j} = 1] = \frac{f}{T}$, where f is the total favorable outcomes and T denotes the total possible outcomes. Since we have only one favorable outcome ($f = 1$), which is $L_{i,j}$, and the total possible outcomes equal to the total unmonitored lines, which is $T = o_i - k_m$, we have $Pr(\mathscr{Z}) = \frac{1}{o_i - k_m}$. Thus, the maximum number of pre-monitored lines can be $k_m = c_i - 1$, as at least 1 current channel has to be available for monitoring another line. Therefore, $Pr(\mathscr{Z})$ becomes $\frac{1}{o_i - c_i + 1}$, where c_i is the total number of channels, as stated in Section II. Setting $c_i = 1$, which is the practical case with most field PMUs, $Pr(\mathscr{Z}) = \frac{1}{o_i}$, which could be very less for a node with high incidence. *To address this, we formulate a weighted incidence problem, with different line weights based on their importance.*

A. Formulation of Multi-attribute Data Pruning Problem

Let the total nodes of interest be numbered $\mathscr{N} = N_1, \cdots, N_S$, the direct measured nodes be numbered $\mathscr{N}_d = D_1, \cdots, D_W$, and the pseudo-measured nodes as $\mathscr{N}_{pm} = P_1, \cdots, P_M$, s.t. $\|\mathscr{N}\| = S$, $\|\mathscr{N}_d\| = W$, $\|\mathscr{N}_{pm}\| = M$, and $W + M = S$. Each of these PMUs take h measurements, with the lth measurement for jth element of these sets represented as x_{l,N_j}, x_{l,D_j}, and x_{l,P_j} respectively. Further, let $\mathscr{X}_{i,D_j} = \{x^i_{1,D_j}, x^i_{2,D_j}, \cdots, x^i_{h,D_j}\}^T$ be the ith sample of the h measured attributes monitored by the PMU at the direct monitored node $D_j \in \mathscr{N}_d$. Consider estimating R time samples for the h attributes measured by the PMUs, s.t. $i = 1, \cdots, R$ and $S_a = \{\nu | \nu \in 1, \cdots, h\}$ is the attribute index set, where ν is the attribute running index.

The prediction for the ith sample $\hat{\mathscr{X}}_{i,D_j} = [\hat{x}^i_{1,D_j}, \cdots, \hat{x}^i_{h,D_j}]^T$ is $\hat{\mathscr{X}}_{i,D_j} = \text{diag}\left(\omega^T_{\mathscr{X}_{i,D_j}} \Phi_{\mathscr{X}_{i,D_j}}\right) + \underline{\mathbb{b}}_{i,D_j}$, where $diag(M)$ forms a vector from the diagonal entries of matrix M with their position in the vector v given by their row or column index in the matrix M, $\underline{\mathbb{b}}_{i,D_j}$ is the $h \times 1$ attribute bias vector, $\omega_{\mathscr{X}_i}$ and $\Phi_{\mathscr{X}_i}$ are the non-linear mapping matrix from input to feature space and the weight matrix for different attributes required for the estimate of ith attribute sample measured at the D_jth direct monitored node [40]. All the rows and columns in $\omega^T_{\mathscr{X}_i}$ and $\Phi_{\mathscr{X}_i}$ are zero padded with the number of zeros $n_0 = d_{\max} - d_p$, where d_p is the number of elements in the pth row or column of $\omega_{\mathscr{X}_i}$ and $\Phi_{\mathscr{X}_i}$ matrices respectively, and $d_{\max} = \max\{d_1, \cdots, d_h\}$. It is notable that d_ν is the number of lag samples used to tune the SVR hyper-parameters for the estimation of the ith sample of νth attribute.

From the standard theory of SVR, we know that minimizing the weights, i.e., $w_{\mathscr{X}^\nu_i, D_j}$, correspond to minimizing the magnitude of the normal vector to the surface that is being approximated, resulting in a solution with optimum fit on the given dataset [41]. Therefore, the optimum weights are obtained using the following optimization problem:

$$\begin{aligned}(\mathbf{P}_1): \min[&\frac{1}{2}\|w_{\mathscr{X}^\nu_{i,D_j}}\|^2 + \Upsilon^\nu \sum_{i=1}^{R}(\theta^\nu_{i,D_j} + \theta^{*\nu}_{i,D_j})] \\ \text{s.t. } \mathbf{C}_1\text{: } &\mathscr{X}^\nu_{i,D_j} - \hat{\mathscr{X}}^\nu_{i,D_j} \leq \epsilon_{\nu,D_j} + \theta^\nu_{i,D_j}\ ,\ \theta^\nu_{i,D_j} \geq 0 \\ \mathbf{C}_2\text{: } &\hat{\mathscr{X}}^\nu_{i,D_j} - \mathscr{X}^\nu_{i,D_j} \leq \epsilon_{\nu,D_j} + \theta^{*\nu}_{i,D_j}\ ,\ \theta^{*\nu}_{i,D_j} \geq 0\end{aligned} \tag{1}$$

where ϵ_ν is the error tolerance for the νth attribute, and θ^ν_{i,D_j}, $\theta^{\nu*}_{i,D_j}$ are the slack variables that are introduced to ensure feasibility of $\mathbf{C}_1$ and $\mathbf{C}_2$, respectively. Therefore, the slack variables must be strictly non-negative [42]. Also, Υ^ν is the trade-off factor in the curvature of $\omega_{\mathscr{X}^\nu_i}$ to θ^ν_i for the νth attribute in $\mathscr{X}^\nu_{i,D_j}$. Since the optimization problem in (1) is convex, we use the standard optimization approach of obtaining its dual. Thus, the dual of (1) is given as

$$\begin{aligned}(\mathbf{P}_2): \min[&\frac{1}{2}\sum_{i,j=1}^{R}(\pi^\nu_{i,D_l} - \pi^{*\nu}_{i,D_l})(\pi^\nu_{j,D_l} - \pi^{*\nu}_{j,D_l})\langle\phi^\nu(\mathscr{X}^\nu_{i,D_l}), \phi^\nu(\mathscr{X}^\nu_{j,D_l})\rangle \\ &+ \epsilon\sum_{i=1}^{R}(\pi^\nu_{i,D_l} + \pi^{*\nu}_{i,D_l}) + \sum_{i=1}^{R}\mathscr{X}^\nu_{i,D_l}(\pi^\nu_{i,D_l} - \pi^{*\nu}_{i,D_l})], \text{ s.t.} \\ \mathbf{C}_3: &\sum_{i=1}^{R}(\pi^\nu_{i,D_l} - \pi^{*\nu}_{i,D_l}) = 0; \pi^\nu_{i,D_l}, \pi^{*\nu}_{i,D_l} \in [0, \Upsilon^\nu]\end{aligned}$$

where $i, j = 1, \cdots, R$ and π^ν_{i,D_l} are the Lagrange multipliers. Replacing $\langle\phi^\nu(\mathscr{X}^\nu_i), \phi^\nu(\mathscr{X}^\nu_j)\rangle$ with a radial basis kernel, we

get

$$\hat{\mathscr{X}}^{\nu}_{i,D_l} = \sum_{i,j=1}^{R} (\pi^{\nu}_{i,D_l} - \pi^{*\nu}_{i,D_l}) \exp(-\beta \| \mathscr{X}_i^{\nu} - \mathscr{X}_j^{\nu} \|)^2 + \mathbb{b}^{\nu}_{i,D_l}.$$

The multi-attribute data pruning approach proposed here precludes the requirement of communicating all of the PMU data to the local PDC; instead, using multivariate SVR technique, a very small fraction is transmitted and the redundant data is dropped. Once the SVR model is constructed at the PDC-end, the PDC is capable of estimating the actual grid data within a predefined tolerable error bound. With this data pruning approach, the PMU-to-PDC data communication occurs infrequently, for the purpose of SVR model retraining at the PDC. This proactive availability of grid health data at the PDC by the virtue of SVR-based data estimation enables predictive event diagnosis, load modeling and forecasting, improved state estimation, etc., which is otherwise not possible in an event-based PMU data communication framework. Therefore, the proposed strategy is more realistic and capable of facilitating a real-time system monitoring provision by the PDC, while utilizing only a very limited fraction of communication resources. The next subsection outlines the modeling of SEP.

B. Mathematical Modeling of SEP

From Section II, we know $\tilde{x}^t_{i,D_j} = x^t_{i,D_j} + \Delta x^t_{i,D_j}\ \forall j \in \mathscr{N}_d$, and $i \in 1, \cdots, h$. The time index t is dropped in the further analysis for brevity. This section analyzes the SEP in the pseudo-measurements due to their estimation based on the distorted direct measurements at the PDC.

Lemma 1. *SEP to the νth pseudo-measurement due to the distorted reconstruction of the direct measurements at the PDC is given by $\boldsymbol{\theta}_\nu = \mathbf{A}_\nu^T \mathbf{e}$, where $\boldsymbol{\theta}_\nu$ is the SEP in the νth pseudo-measurement across M pseudo-monitored nodes, s.t. $\boldsymbol{\theta}_\nu = [\Delta x_{\nu,1}, \Delta x_{\nu,2}, \cdots, \Delta x_{\nu,M}]^T$, and $\mathbf{A}_\nu = [\mathbf{A}_{1,\nu}, \mathbf{A}_{2,\nu}, \cdots, \mathbf{A}_{W,\nu}]^T$ is the SEP matrix for the νth pseudo-measurement, with $\mathbf{e} = [\mathbf{e}_1, \mathbf{e}_2, \cdots, \mathbf{e}_W]^T$ being the joint measurement error vector.*

Proof. See Appendix A □

Let the error vector be $\mathbf{e} = [\mathbf{e}_{D_1}, \cdots, \mathbf{e}_{D_W}]^T$, where $\mathbf{e}_{D_j} = [\Delta x_{1,D_j}, \cdots, \Delta x_{h,D_j}]^T$. Thus, using Lemma 1 we have

$$\mathbf{e} = (\mathbf{A}_\nu \mathbf{A}_\nu^T)^{-1} \mathbf{A}_\nu \boldsymbol{\theta}_\nu \ ; \forall \nu \in \{1, \cdots, h\}. \tag{2}$$

Since error has to be maintained within a tolerance at all pseudo-monitored nodes for all attributes, with the error tolerance in the νth attribute given by ϵ_ν. We must have $\boldsymbol{\theta}_\nu \leq \epsilon_\nu \mathbb{1}$, where ϵ_ν is a predefined error threshold in the νth attribute estimation, and $\mathbb{1} = [1, \cdots, 1]^T$ is a vector of ones of appropriate dimension. Therefore, the error tolerance at the direct monitored nodes against νth pseudo-measurement is $\mathbf{e} = (\mathbf{A}_\nu \mathbf{A}_\nu^T)^{-1} \mathbf{A}_\nu \epsilon_\nu \mathbb{1}$, $\forall \nu \in \{1, \cdots, h\}$. Thus, by choosing $\epsilon_{\min} = \min_{\nu \in \{1, \cdots, h\}} \epsilon_\nu$, an upper bound on $\mathbf{e}$ is defined as

$$\mathbf{e} \leq (\mathbf{A}_\nu \mathbf{A}_\nu^T)^{-1} \mathbf{A}_\nu \epsilon_{\min} \mathbb{1}. \tag{3}$$

Therefore, the error tolerance of the νth attribute for the jth direct-monitored node is the $\{\nu + (j-1)h\}$th element of error vector defined in (3), given as $\epsilon_{\nu,D_j} = \mathbf{e}\{\nu + (j-1)h\}$. A system-aware multi-attribute real-time data pruning optimization problem based on (1) can thus be formulated as

$$\begin{aligned} (\mathbf{P}_3): \min [\frac{1}{2} \| w_{\mathscr{X}^{\nu}_{i,D_j}} \|^2 + \Upsilon^{\nu} \sum_{i=1}^{R} (\theta^{\nu}_{i,D_j} + \theta^{*\nu}_{i,D_j})] \\ \text{s.t. } \mathbf{C}_4\text{: } \mathscr{X}^{\nu}_{i,D_j} - \hat{\mathscr{X}}^{\nu}_{i,D_j} \leq \mathbf{e}\{\nu + (j-1)h\} + \theta^{\nu}_{i,D_j} \\ \mathbf{C}_5\text{: } \hat{\mathscr{X}}^{\nu}_{i,D_j} - \mathscr{X}^{\nu}_{i,D_j} \leq \mathbf{e}\{\nu + (j-1)h\} + \theta^{*\nu}_{i,D_j} \\ \text{and, } \theta^{\nu}_{i,D_j}, \theta^{*\nu}_{i,D_j} \geq 0. \end{aligned} \tag{4}$$

(4) is solved as in Section III-A, resulting in a system-aware data pruning due to the system-aware bounds in $\mathbf{C}_4$ and $\mathbf{C}_5$.

Dissecting Lemma 1, error contribution due to the distorted reconstruction of the ith direct measurement in the estimation of νth pseudo-measurement at node P_j is $\nabla f_{P_j,D_i,\nu}(\mathbf{X}_{D_i})$. This measure helps in defining the sensitivity of a node based on its ability to impair a pseudo-measurement, thus affecting the PMU placement strategy. We define the most sensitive parameter in the νth attribute estimation at node P_j, as the one with maximum aggregate gain through all measured nodes, thus contributing the maximum error fraction in x_{ν,P_j}.

Definition 1. *For all direct measured nodes from set $\mathscr{N}_d$, the node with maximum sensitivity corresponding to the νth measurement at P_j is given by $D_i = \{D_i | i \rightarrow \max_{i \in \mathscr{D}_i} \nabla f_{P_j,D_i,\nu}(\mathbf{X}_{D_i})\}$, and the most sensitive parameter is given by $x_k = \{x_k | k \rightarrow \max_{k \in \{1,\cdots,h\}} \sum_{i=1}^{W} \frac{\partial f_{P_j,D_i,\nu}(\mathbf{X}_{D_i})}{\partial x_{k,D_i}}\}$.*

Using Def. 1, b_i is written as

$$b_i = \begin{cases} \frac{\sum_{\forall P_j} \sum_{\forall \nu} \|\nabla f_{P_j,D_i,\nu}(\mathbf{X}_{D_i})\|}{\sum_{\forall P_j} \sum_{\forall D_i} \sum_{\forall \nu} \|\nabla f_{P_j,D_i,\nu}(\mathbf{X}_{D_i})\|}, & i \in \mathscr{N}_d \\ \frac{\sum_{\forall D_j} \sum_{\forall \nu} \|\nabla f_{P_i,D_j,\nu}(\mathbf{X}_{D_j})\|}{\sum_{\forall P_i} \sum_{\forall D_j} \sum_{\forall \nu} \|\nabla f_{P_i,D_j,\nu}(\mathbf{X}_{D_j})\|}, & i \in \mathscr{N}_{pm} \end{cases} \tag{5}$$

C. Formulation of Optimal PMU Placement Problem

This subsection proposes the joint optimal PMU placement strategy in a resource utilization efficient smart grid communication scenario. The objective of this formulation is to optimally place the PMUs to make the system topologically observable. The optimization problem is formulated as

$$\begin{aligned} (\mathbf{P}_4)\text{: Min}_{\mathbf{U}}\ \left\{\mathbf{U}^T \mathbf{C}_P \mathbf{U} + \mathbf{G}(\mathbf{U})^T \mathbf{V} \mathbf{G}(\mathbf{U})\right\} \\ (\mathbf{P}_5)\text{: Max}_{\mathbf{U}}\ \mathbf{U}^T \mathbf{F}(\mathbf{U}) \mathbf{U} \\ \text{s.t. } \mathbf{C}_6\text{: } 0 \leq u_i \leq 1,\ \forall u_i \in \mathbf{U} \\ \text{and, } (\mathbf{P}_6)\text{: Max}_{\mathbf{U}}\ \mathbb{1}^T_{n \times 1} \mathbf{A}_w \mathbf{U} \text{ s.t., } \mathbf{C}_7\text{: } \mathbf{U} \in \mathbf{U}^* \end{aligned} \tag{6}$$

where $\mathbf{U}$ is the PMU placement vector, $\mathbf{C}_p$ is the diagonal PMU cost matrix, with the ith diagonal element denoting the cost of the PMU installed at node i, $\mathbf{G}(\mathbf{U})$ is the diagonal polynomial observability constraint matrix, $\mathbf{V}$ is the diagonal observability weight matrix, and $\mathbf{A}_w$ is the weighted grid incidence matrix. $(\mathbf{P}_5)$ optimizes the total communication bandwidth saving for the grid, thus taking care of smart PMU communication, with $\mathbf{F}(\mathbf{U})$ denoting the average communication bandwidth saving for the PMU installed at the ith bus $\forall i = 1, \cdots, S$. $(\mathbf{P}_6)$ maximizes the total measurement redundancy for the grid on the PMU placement set $\mathbf{U}^*$ found

by optimizing $(\mathbf{P}_4)$ and $(\mathbf{P}_5)$. Further, $(\mathbf{P}_4)$-$(\mathbf{P}_6)$ are convex due to their quadratic form. Thus an optimum is guaranteed.

Remark 2. *In the optimization formulation in* (6)*, the objective functions* $(\mathbf{P}_4)$ *and* $(\mathbf{P}_5)$ *are constrained by* $\mathbf{C}_6$*, while* $(\mathbf{P}_6)$ *is constrained by* $\mathbf{C}_7$*. Furthermore, since all these objective problems* $(\mathbf{P}_4)$-$(\mathbf{P}_6)$ *and constraints* $\mathbf{C}_6$ *and* $\mathbf{C}_7$ *have the common decision variable* $\mathbf{U}$*, all these objective functions must be optimized together to achieve fairness, i.e., to avoid trading one optimization solution for optimizing another.*

For the ith node, each incidence line shares an importance of $\frac{b_i}{o_i}\mathbb{R}(L_{i,j}=1)\ \forall j \in \mathscr{I}_i$. $\mathbb{R}(L_{i,j}=1)$ is a binary indicator variable which takes 1 iff node i is connected to j, $\mathbb{1}_{S\times 1}$ is an S dimensional vector of ones and $\mathscr{I}_i$ is the incidence node set for the ith node. Therefore, the (m,n)th entry of $\mathbf{A}_w$ is given by $\mathbf{A}_w(m,n) = \frac{b_m}{o_m}\mathbb{R}(L_{m,n}=1)$. A joint optimization problem from (6) is formulated as given below.

$$\begin{aligned}&(\mathbf{P}_7)\text{: Min}_{\mathbf{U}}\ \big\{w_1(\mathbf{U}^T\mathbf{C}_P\mathbf{U}+\mathbf{G}(\mathbf{U})^T\mathbf{V}\mathbf{G}(\mathbf{U}))\\ &-w_2\mathbf{U}^T\mathbf{F}(\mathbf{U})\mathbf{U}\big\}\text{, s.t. } \mathbf{C}_6\\ &(\mathbf{P}_6)\text{: Max}_{\mathbf{U}}\ \mathbb{1}_{n\times 1}^T\mathbf{A}_w\mathbf{U}\text{, s.t. } \mathbf{C}_7\end{aligned} \tag{7}$$

where w_1 and w_2 are binary indicator variables. For $w_2=0$, the optimization in $(\mathbf{P}_7)$ reduces to conventional PMU placement without data pruning, whereas $w_2=1$ corresponds to the proposed joint optimal PMU placement and system-aware data pruning. Since $u_i \in \mathbf{U}$ is continuous, we set high node observability weights to push u_i to the extreme limits. The observability polynomial for node i is given by $\mathbf{g}(\mathbf{U})_i = (\sigma_i - u_i - \sum_{j\in\mathscr{I}_i} u_j)$, where σ_i is the redundancy order for bus i. It is noted that $\mathbf{g}(\mathbf{U})_i$ is zero, when σ_i number of incident nodes to node i, inclusive of the ith node itself, have PMUs installed on them. Thus, with $\sigma_i=1$, the observability polynomial for the ith node is zero if at least one incident node to node i, including the ith node, has a PMU monitoring it. Therefore, using this metric in (7), we get

$$\begin{aligned}&(\mathbf{P}_8)\text{: Min}_{u_i\forall i\in\{1,\cdots,n\}}\sum_{i=1}^{n}\big\{w_1\big(cu_i^2+v_i\,(\sigma_i-u_i\\ &-\sum_{j\in\mathscr{I}_i}u_j)^2\big)-w_2f_i(\mathbf{U})u_i^2\big\}\text{, s.t. } \mathbf{C}_6 \text{ and } (\mathbf{P}_6).\end{aligned} \tag{8}$$

where the summations over i result from opening the quadratic formulations $\mathbf{U}^T\mathbf{C}_P\mathbf{U}$, $\mathbf{G}(\mathbf{U})^T\mathbf{V}\mathbf{G}(\mathbf{U}))$, and $\mathbf{U}^T\mathbf{F}(\mathbf{U})\mathbf{U}$.

Remark 3. *It is notable that optimizing* $(\mathbf{P}_6)$ *subject to* $\mathbf{C}_7$ *is a contention resolution proposition for choosing between multiple optimal solutions from* $(\mathbf{P}_7)$*. The final solution to the optimization set* $(\mathbf{P}_4)$-$(\mathbf{P}_5)$ *must satisfy* $(\mathbf{P}_6)$*, i.e., must maximize* $\mathbb{1}_{n\times 1}^T\mathbf{A}_w\mathbf{U}$*. Since* $(\mathbf{P}_6)$ *limits the solution set for the objective function* $(\mathbf{P}_8)$*,* $(\mathbf{P}_6)$ *is imposed as a constraint in* (8)*. Therefore, using* $(\mathbf{P}_6)$ *as a constraint on the solutions obtained from optimizing* $(\mathbf{P}_4)$ *and* $(\mathbf{P}_5)$ *jointly optimizes the problem set* $(\mathbf{P}_4)$-$(\mathbf{P}_6)$*.*

IV. IEEE 6-Bus Power System Test Case

In this section, an IEEE 6-bus system is considered for the SEP analysis. For the purpose of observing the complete grid, we use the conventional optimal PMU placement scheme. The analysis presented here is extended to propose the joint optimal PMU placement and data pruning strategy. Let the direct measurements at buses 4 and 5 be E_4, δ_4, I_{41}, ϕ_{41} and E_5, δ_5, I_{65}, ϕ_{65}, respectively. These measurements act as bases in the estimation of measurements at the remaining buses.

Theorem 1. *The error propagated in voltage magnitude across all the pseudo-monitored nodes is given as*

$$\mathbf{\Delta E} = \mathbf{J}_1\mathbf{\Delta E}_P + \mathbf{J}_2\mathbf{\Delta\delta}_P + \mathbf{J}_3\mathbf{\Delta I}_P + \mathbf{J}_4\mathbf{\Delta\phi}_P$$

where $\mathbf{\Delta E}_P$*,* $\mathbf{\Delta\delta}_P$*,* $\mathbf{\Delta I}_P$*, and* $\mathbf{\Delta\phi}_P$ *are the reconstruction errors in voltage magnitude, voltage phase, current magnitude, and current phase bases respectively.* $\mathbf{J}_k$*, for* $k\in\{1,\cdots,4\}$ *are the respective voltage error gain matrices.*

Proof. See Appendix B. □

Theorem 2. *The error propagated in current magnitude through all pseudo-monitored lines in the grid is given as*

$$\mathbf{\Delta I} = \mathbf{H}_1\mathbf{\Delta E}_P + \mathbf{H}_2\mathbf{\Delta\delta}_P + \mathbf{H}_3\mathbf{\Delta I}_P + \mathbf{H}_4\mathbf{\Delta\phi}_P$$

where all notations are as defined in Theorem 1, and $\mathbf{H}_k$*,* $k\in\{1,\cdots,4\}$ *are current error gain matrices.*

Proof. See Appendix C. □

We continue the error propagation analysis in the power estimates in an IEEE 6-bus system. The directly measured complex powers are S_{65} and S_{41} with the active and reactive part given as (P_{65}, Q_{65}) and (P_{41}, Q_{41}). The error propagated to active power pseudo-measurements is given by Theorem 3.

Theorem 3. *The error observed in pseudo-monitored active power flowing in the grid is given by*

$$\mathbf{\Delta P} = \mathbf{R}_1\mathbf{\Delta E}_P + \mathbf{R}_2\mathbf{\Delta\delta}_P + \mathbf{R}_3\mathbf{\Delta I}_P + \mathbf{R}_4\mathbf{\Delta\phi}_P$$

where $\mathbf{R}_k$*, s.t.* $k\in\{1,\cdots,4\}$ *are power error gain matrices.*

Proof. See Appendix D. □

The error in reactive power pseudo-measurements is defined by Theorem 4.

Theorem 4. *The error observed in pseudo-monitored reactive power flow in the grid is given by*

$$\mathbf{\Delta P} = \mathbf{T}_1\mathbf{\Delta E}_P + \mathbf{T}_2\mathbf{\Delta\delta}_P + \mathbf{T}_3\mathbf{\Delta I}_P + \mathbf{T}_4\mathbf{\Delta\phi}_P$$

where $\mathbf{T}_k$*, s.t.* $k\in\{1,\cdots,4\}$ *are power error gain matrices.*

Proof. See Appendix E. □

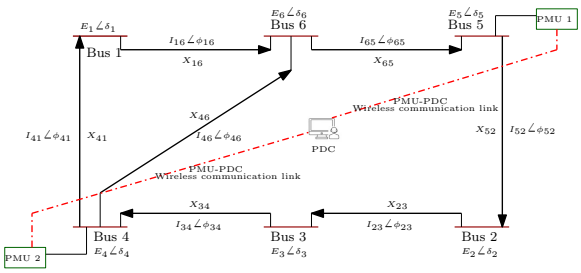

Fig. 2: Line diagram of IEEE 6-bus standard power system.

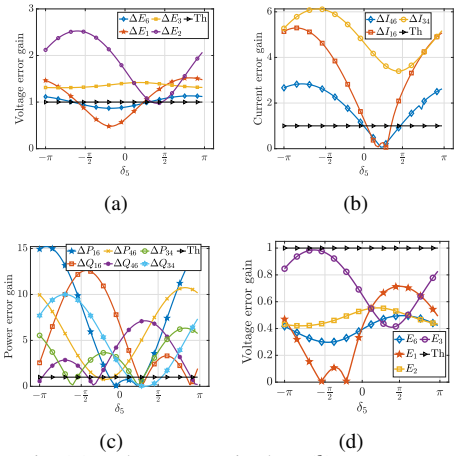

Fig. 3: SEP in (a) voltage magnitudes, (b) current magnitudes, (c) power magnitudes in system-agnostic error settings; SEP in (d) voltage magnitude in system-aware error settings; with δ_5.

Remark 4. *It is notable that our attribute tolerance thresholds are upper bounded by the allowable per-unit magnitude deviations as per the 'Indian Electricity Grid Code (IEGC)'.*

V. Results and Discussions

This section contrasts the performance of the proposed joint optimal PMU placement and system-aware data pruning approach with the most competitive state-of-the-art approaches. The key performance indices used to quantify the the performances are defined in Section V-A. For actual deployment solutions, we have considered practical line PMUs (from Vizimax: https://www.vizimax.com/) with 1 input current channel. These numerical results are shown in Tables II-VII.

A. Key Performance Indices

For the performance analysis of the proposed system-aware data pruning framework, following indices are defined:

1) Normalized root mean square error (nRMSE): For νth attribute, $nRMSE = \frac{\sum_{\nu=1}^{h} ||\varepsilon_\nu/\sqrt{l}||}{h}$, with $\varepsilon_\nu = x_{\nu,D_j} - \tilde{x}_{\nu,D_j}$.

2) Communication bandwidth saving: It is defined as the percentage of actual data that were not transmitted within a system specific error tolerance ε constrained by the SVR tube.

3) Attribute error gain: Attribute error gain $G_{i,j}$ in the ith attribute, is the change in the estimation error for the ith attribute at a pseudo-monitored node as one of the system attribute x_j varies. Mathematically, $G_{i,j} = \lim_{\mathscr{D}x_j \to 0} \frac{\mathscr{D}(\Delta x_i)}{\mathscr{D}x_j}$ $\forall\{i,j\} \in \{1,\cdots,h\}$, where $\mathscr{D}y$ represents change in y.

4) Observability loss: Observability loss under a grid adversity is defined as the ratio of total nodes estimated within the predefined threshold, using the reconstructed PMU data at the data collector, to the total number of grid nodes.

B. SEP Analysis on IEEE 6-Bus System

Figs. 3(a)-3(d) show the impact of system state on the attribute error gain $G_{i,j}$ with δ_5. From Figs. 3(a)-3(c), it can be observed that with system agnostic error settings, the error gains in voltage, current, and power magnitudes across pseudo-monitored nodes exceed the threshold as the value of δ_5 state varies. Further, it can be inferred that the impact varies with change in system states. It can also be noted that the entire system space is not equally vulnerable. Similar conclusions can be drawn for error gain variation with change in other state values, such as, voltage, current, frequency, ROCOF etc. This gives a valuable insight into the need for a system-aware data pruning, thereby assuring tolerance within range, so as to not have misleading attribute estimations. Fig. 3(d) shows the variation of voltage error gain with system-aware optimum error tolerance settings against the possible range of δ_5. The plots show that, with system-aware tolerance setting, the SEP always stays below the threshold – marked by the right-arrowed line. For brevity, we have excluded system-aware SEP plots for other attributes. However, using Theorem 1-4, similar analysis can be extended for other attributes. Thus, (4), guarantees an upper bound on SEP for all attributes.

TABLE I: Performance indices.

Avg. tube width, ϵ	Tol., ε_{th}	Corr. th., $\mathbf{c}_t$	Lag, d	nRMSE
10^{-3}	10^{-1}	0.7	5	3.46×10^{-5}

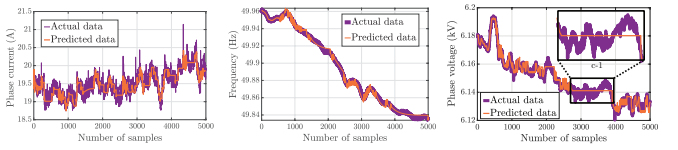

Fig. 4: Comparison of actual versus predicted samples: (a) phase current; (b) frequency; (c) phase voltage.

C. Conventional Optimal PMU Placement and Data Pruning

The algorithm in [40] was implemented on the setup described in Remark 1 with optimal hyper-parameters' settings in Table I, and the predictions for all attributes were done for the direct monitored node. It is observed from Fig. 4 that the actual samples closely match the estimated values. Table II shows the impact of node-level data pruning on the conventional PMU placement strategy. It is observed that each PMU is able to reach the maximum prunability, thus achieving maximum communication bandwidth saving. However, the average node estimation error crosses the defined threshold because of the system-agnostic setup. Also, it is notable from observability loss in Table II that, the aggregate grid observability drops under single PMU loss (SPL) and single line loss (SLL). Furthermore, due to the system agnostic data pruning, the bandwidth (BW) consumption under node-level data pruning during SPL/SLL stays unaltered. However, as a consequence of node-level data pruning, the reconstruction error increases.

Table III presents the analysis of system-aware data pruning formulation with conventional PMU placement. It can be noted that the prunability per PMU is highest for the IEEE 6-bus system. Also, the maximum prunability decreases as the system size grows, increasing the average bandwidth consumption. Therefore, it is concluded that the grid size and node connectivity play a crucial role in optimal PMU placement and optimum data pruning. When a system-aware data pruning is employed in conventional PMU placement setup, a similar

TABLE II: Performance with conventional PMU placement and node-level optimum data pruning for different IEEE systems

Bus syst.	Optimal PMU locations	Opt. prun-ability %	BW consumption			Average node estimation error			Exec. time (s)	Obs. loss	
			Normal	SPL	SLL	Normal	SPL	SLL		SPL	SLL
6	4, 5	95.5	0.138	0.069	0.138	7.9×10^{-2}	0.241	0.173	6.14	0.667	0.5
14	2, 6, 7, 9	95.5	0.288	0.216	0.288	9.8×10^{-2}	0.1	0.1	15.57	0.386	0.371
30	1, 7, 8, 10, 11, 12, 18, 23, 26, 30	95.5	0.727	0.654	0.727	3.7×10^{-2}	0.052	0.023	38.62	0.267	0.233
57	2, 6, 10, 12, 19, 22, 25, 27, 32, 36, 41, 45, 46, 49, 52, 55, 57	95.5	1.389	1.307	1.389	5.6×10^{-2}	0.086	0.077	71.47	0.451	0.417

TABLE III: Performance with conventional PMU placement and system-aware optimum data pruning for different IEEE systems

Bus syst.	Optimal PMU locations	Opt. prun-ability %	BW consumption			Average node estimation error			Exec. time (s)	Obs. loss	
			Normal	SPL	SLL	Normal	SPL	SLL		SPL	SLL
6	4, 5	91.4	0.236	0.472	0.354	3.8×10^{-4}	4.6×10^{-2}	3.9×10^{-3}	6.16	0.652	0.48
14	2, 6, 7, 9	90.3	0.388	1.046	1.005	4.3×10^{-4}	6×10^{-3}	4.7×10^{-3}	15.53	0.373	0.359
30	1, 7, 8, 10, 11, 12, 18, 23, 26, 30	89.1	1.112	4.773	4.165	5.1×10^{-4}	5.7×10^{-4}	5.6×10^{-4}	38.71	0.224	0.217
57	2, 6, 10, 12, 19, 22, 25, 27, 32, 36, 41, 45, 46, 49, 52, 55, 57	82.7	3.410	7.714	6.586	6.4×10^{-4}	9.8×10^{-4}	7.3×10^{-4}	71.39	0.419	0.401

TABLE IV: Performance with joint optimal PMU placement and optimum data pruning for different IEEE systems

Bus syst.	Optimal PMU locations	Opt. prun-ability %	BW consumption			Average node estimation error			Exec. time (s)	Obs. loss	
			Normal	SPL	SLL	Normal	SPL	SLL		SPL	SLL
6	3, 4, 6	95.5	0.185	0.185	0.185	1.2×10^{-5}	1.2×10^{-5}	1.2×10^{-5}	7.07	0.0001	0.0005
14	2, 4, 7, 9, 13	95.5	0.295	0.295	0.295	1.4×10^{-4}	1.4×10^{-4}	1.4×10^{-4}	18.41	0.0001	0.0002
30	1, 2, 5, 6, 9, 10, 12, 17, 19, 22, 24, 25, 27, 29	95.5	0.787	0.787	0.787	1.5×10^{-5}	1.5×10^{-5}	1.5×10^{-5}	47.19	0.0001	0.0001
57	1, 2, 4, 6, 9, 12, 15, 19, 20, 22, 24, 26, 29, 30, 31, 32, 35, 36, 41, 45, 46, 50, 51, 53, 56, 57	95.5	1.583	1.583	1.583	1.4×10^{-5}	1.4×10^{-5}	1.4×10^{-5}	84.76	0.0001	0.0003

observability loss is noted from Table III, with a corresponding increase in bandwidth consumption. This results from the requirement of higher redundancy in the data monitored by the PMUs, to compensate for a PMU loss, or higher overall data cardinality compensating the line loss. Thus, managing the optimum possible observability in the remaining resources. Therefore, we conclude that increasing the data redundancy helps in node estimation within the desired error threshold.

D. Joint Optimal PMU Placement and Data Pruning Analysis

From the joint optimal PMU placement and data pruning strategy ($w_2 = 1$) in Table IV, it can be observed that the number of PMUs as well as their locations are different from the ones obtained using the conventional approach ($w_2 = 0$). With $w_2 = 1$, the maximum prunability per PMU reaches up to 95.5%, thereby significantly decreasing the total bandwidth consumption without compromising on the error tolerance. In contrast, referring to Table III, the optimal PMU placement from the conventional strategy results in an inefficient PMU data compressibility for the same order of error tolerance.

Thus, it is concluded that in a data communication-aware system monitoring, just observability-based PMU placement is insufficient. Though joint optimal PMU placement adds some redundancy on the optimum number of PMUs required for efficient grid monitoring, the bandwidth consumption is significantly reduced. Compared to the node-level data pruning under normal grid conditions, which does not exploit inter-PMU data correlation, the additional average communication bandwidth saving is $\approx 34\%$, while limiting the data reconstruction error within the same tolerable limit 10^{-3}. Similarly, under normal system operating conditions, when compared to the system-aware data pruning in conventional placement framework, the additional average communication bandwidth saving is $\approx 32\%$ for the same tolerable data estimation error. Furthermore, one significant observation results from the impact on system observability under SPL and SLL. Since the proposed optimal PMU placement provides inherent redundancy, the observability loss is ≈ 0, with no significant rise in bandwidth consumption. *It is notable that under any setting of w_1 and w_2, all the PMUs have different prunability based on the node sensitivity in Def. 1.*

TABLE V: Performance of conventional PMU placement and system-aware data pruning in real power networks; N_{PMU}: Number of PMUs

System [N_{PMU}]	Optimal PMU locations	BW cons.	Average node estimation error	Execution time (s)
A [13]	2, 6, 9, 13, 14, 17, 19, 20, 22, 23, 25, 29, 32	2.38B	1.37×10^{-4}	52.852
B [26]	26, 30, 31, 33, 34, 35, 40, 41, 43, 44, 46, 47, 49, 52, 55, 57, 58, 59, 60, 62, 65, 66, 67, 68, 69, 71	4.59B	3.11×10^{-4}	100.705
C [71]	4, 6, 9, 16, 18, 19, 23, 28, 36, 39, 43, 45, 56, 57, 60, 61, 62, 72, 78, 88, 93, 95, 97, 98, 99, 101, 102, 106, 108, 111, 115, 117, 126, 129, 133, 134, 138, 143, 147, 153, 154, 156, 160, 163, 164, 169, 177, 179, 183, 185, 187, 188, 192, 195, 197, 198, 201, 202, 203, 206, 207, 210, 211, 212, 217, 222, 225, 228, 232, 233, 240	15.43B	1.60×10^{-3}	271.193
D [556]	30, 35, 81, 105, 126, 132, 184, 188, 190, 192, 199, 202, 213, 214, 215, 217, 219, 224, 229, 236, 240, 244, 245, 246, 247, 251, 259, 262, 265, 274, 275, 276, 277, 285, 287, 290, 291, 295, 307, 308, 311, 314, 319, 321, 322, 324, 326, 328, 329, 334, 335, 337, 341, 345, 348, 353, 354, 358, 360, 363, 365, 366, 371, 373, 386, 391, 394, 399, 404, 411, 417, 418, 419, 421, 425, 428, 432, 439, 443, 445, 446, 448, 460, 463, 464, 466, 468, 472, 474, 476, 477, 479, 481, 488, 489, 493, 494, 498, 499, 510, 511, 512, 515, 523, 525, 526, 527, 529, 530, 540, 550, 551, 556, 567, 570, 571, 579, 584, 591, 592, 601, 604, 609, 613, 615, 618, 619, 622, 635, 638, 643, 644, 649, 651, 655, 658, 660, 661, 670, 672, 675, 679, 685, 687, 689, 690, 692, 694, 696, 698, 703, 707, 709, 710, 712, 713, 717, 722, 724, 726, 727, 740, 741, 744, 748, 750, 754, 755, 763, 765, 771, 773, 775, 778, 782, 785, 792, 794, 795, 796, 798, 811, 813, 814, 815, 817, 819, 820, 821, 826, 827, 832, 834, 839, 850, 857, 858, 859, 869, 870, 871, 878, 883, 892, 905, 912, 913, 919, 922, 929, 947, 950, 961, 964, 967, 968, 973, 975, 978, 985, 988, 994, 995, 996, 997, 1005, 1019, 1020, 1024, 1051, 1059, 1063, 1069, 1070, 1082, 1083, 1091, 1092, 1095, 1096, 1097, 1104, 1117, 1120, 1122, 1138, 1140, 1141, 1147, 1149, 1155, 1165, 1168, 1171, 1178, 1182, 1184, 1187, 1190, 1195, 1198, 1201, 1207, 1210, 1216, 1217, 1230, 1232, 1233, 1235, 1245, 1249, 1250, 1251, 1254, 1259, 1261, 1272, 1277, 1284, 1285, 1288, 1292, 1311, 1328, 1335, 1343, 1346, 1351, 1365, 1375, 1387, 1389, 1399, 1415, 1416, 1422, 1424, 1426, 1427, 1435, 1437, 1459, 1460, 1469, 1476, 1483, 1486, 1489, 1505, 1506, 1507, 1512, 1514, 1518, 1523, 1524, 1528, 1531, 1533, 1534, 1535, 1536, 1539, 1540, 1545, 1547, 1550, 1552, 1553, 1556, 1565, 1568, 1575, 1576, 1580, 1585, 1586, 1587, 1589, 1592, 1593, 1595, 1597, 1603, 1604, 1607, 1611, 1616, 1619, 1620, 1622, 1623, 1628, 1630, 1647, 1650, 1652, 1656, 1657, 1658, 1659, 1660, 1662, 1667, 1668, 1669, 1673, 1674, 1680, 1681, 1683, 1684, 1686, 1687, 1690, 1691, 1692, 1696, 1699, 1716, 1717, 1721, 1722, 1723, 1728, 1735, 1745, 1755, 1756, 1760, 1761, 1766, 1772, 1774, 1783, 1787, 1795, 1800, 1806, 1808, 1810, 1814, 1816, 1822, 1825, 1829, 1841, 1843, 1845, 1852, 1862, 1864, 1866, 1867, 1869, 1873, 1882, 1883, 1884, 1885, 1890, 1895, 1901, 1906, 1912, 1915, 1916, 1919, 1920, 1921, 1926, 1933, 1936, 1938, 1940, 1943, 1945, 1951, 1956, 1957, 1961, 1963, 1965, 1970, 1974, 1979, 1982, 1989, 1990, 1996, 1998, 2001, 2003, 2005, 2006, 2018, 2020, 2021, 2022, 2024, 2025, 2037, 2039, 2041, 2042, 2045, 2046, 2047, 2050, 2052, 2054, 2056, 2062, 2086, 2087, 2088, 2093, 2099, 2102, 2105, 2113, 2119, 2124, 2126, 2131, 2135, 2137, 2144, 2154, 2157, 2159, 2166, 2167, 2168, 2170, 2172, 2175, 2176, 2178, 2179, 2180, 2184, 2189, 2190, 2191, 2195, 2196, 2202, 2203, 2207, 2217, 2218, 2223, 2224, 2229, 2232, 2233, 2235, 2242, 2243, 2245, 2251, 2252, 2255, 2261, 2264, 2265, 2267, 2274, 2283, 2290, 2291, 2293, 2294, 2298, 2300, 2310, 2313, 2315, 2316, 2323, 2334, 2337, 2342, 2345, 2346, 2349, 2350, 2352, 2359, 2360, 2372, 2374, 2379, 2380	151.78B	7.17×10^{-4}	2217.681
E [23]	1, 6, 11, 14, 17, 18, 21, 22, 23, 24, 25, 26, 27, 28, 29, 30, 31, 32, 33, 34, 23, 35, 36	4.99B	4.21×10^{-4}	93.739

TABLE VI: Performance of joint optimal PMU placement and data pruning in real power networks; N_{PMU}: Number of PMUs

System [N_{PMU}]	Optimal PMU location(s)	BW cons.	Average node estimation error	Execution time (s)
A [21]	1, 2, 3, 6, 8, 9, 10, 11, 13, 14, 16, 17, 19, 22, 23, 25, 29, 30, 32, 36, 37	1.17B	3.01×10^{-5}	81.582
B [33]	3, 5, 6, 10, 16, 17, 26, 29, 30, 31, 34, 35, 37, 40, 41, 43, 45, 46, 47, 52, 53, 55, 57, 59, 60, 62, 64, 65, 66, 67, 68, 69, 72	1.82B	1.73×10^{-5}	121.232
C [92]	4, 6, 8, 11, 13, 14, 16, 20, 21, 22, 26, 27, 29, 31, 32, 33, 34, 35, 38, 42, 46, 47, 52, 54, 56, 59, 61, 63, 68, 71, 75, 76, 78, 84, 86, 89, 91, 93, 96, 99, 106, 108, 110, 111, 114, 116, 119, 123, 134, 136, 137, 138, 140, 143, 147, 152, 154, 157, 158, 160, 162, 164, 167, 170, 175, 178, 181, 183, 186, 188, 189, 190, 192, 194, 197, 198, 205, 206, 207, 210, 213, 219, 220, 221, 222, 225, 226, 231, 237, 239, 240, 242	4.87B	3.32×10^{-5}	314.132
D [590]	28, 36, 40, 45, 81, 105, 126, 132, 151, 163, 184, 188, 192, 199, 202, 213, 214, 215, 217, 219, 224, 229, 236, 240, 244, 247, 251, 255, 259, 262, 265, 275, 276, 277, 285, 287, 290, 295, 307, 308, 311, 314, 319, 321, 324, 326, 328, 329, 334, 335, 337, 341, 345, 348, 354, 358, 360, 363, 365, 366, 371, 373, 386, 391, 394, 399, 408, 411, 417, 418, 419, 421, 425, 428, 432, 439, 443, 445, 446, 448, 455, 460, 463, 464, 466, 468, 472, 474, 476, 477, 479, 481, 482, 483, 488, 489, 493, 494, 498, 499, 505, 507, 510, 511, 512, 515, 523, 525, 526, 527, 529, 530, 540, 550, 551, 556, 567, 570, 571, 573, 579, 584, 591, 592, 601, 604, 609, 613, 615, 618, 619, 622, 635, 638, 643, 644, 648, 649, 651, 655, 658, 660, 661, 670, 672, 675, 679, 683, 685, 687, 689, 692, 694, 696, 698, 703, 707, 709, 710, 713, 717, 722, 724, 726, 727, 730, 734, 738, 740, 741, 743, 744, 748, 750, 752, 754, 755, 757, 761, 763, 765, 770, 771, 773, 775, 778, 782, 785, 792, 794, 795, 796, 798, 805, 811, 813, 814, 815, 817, 819, 820, 821, 826, 831, 832, 834, 839, 840, 847, 850, 857, 858, 859, 869, 870, 871, 878, 883, 892, 905, 912, 913, 919, 922, 929, 947, 950, 954, 961, 964, 968, 973, 975, 978, 985, 988, 994, 995, 996, 997, 1005, 1011, 1019, 1020, 1024, 1037, 1042, 1051, 1059, 1063, 1069, 1070, 1082, 1083, 1091, 1092, 1095, 1096, 1097, 1104, 1117, 1120, 1122, 1138, 1140, 1141, 1147, 1149, 1155, 1165, 1168, 1171, 1178, 1182, 1184, 1187, 1190, 1195, 1198, 1201, 1207, 1210, 1216, 1217, 1222, 1230, 1232, 1235, 1245, 1249, 1250, 1251, 1254, 1259, 1261, 1272, 1277, 1284, 1285, 1288, 1292, 1311, 1328, 1335, 1343, 1346, 1351, 1365, 1375, 1387, 1389, 1399, 1415, 1416, 1422, 1424, 1426, 1427, 1435, 1437, 1459, 1460, 1469, 1476, 1483, 1486, 1489, 1493, 1505, 1507, 1512, 1514, 1518, 1523, 1524, 1528, 1531, 1533, 1534, 1535, 1536, 1539, 1540, 1545, 1547, 1550, 1552, 1553, 1556, 1565, 1568, 1575, 1576, 1580, 1585, 1586, 1587, 1589, 1592, 1593, 1595, 1597, 1603, 1604, 1607, 1611, 1616, 1619, 1620, 1622, 1623, 1628, 1630, 1647, 1650, 1652, 1656, 1657, 1659, 1660, 1662, 1667, 1668, 1669, 1673, 1674, 1680, 1681, 1683, 1684, 1686, 1687, 1690, 1691, 1692, 1696, 1699, 1711, 1716, 1717, 1721, 1722, 1723, 1728, 1735, 1745, 1748, 1755, 1760, 1761, 1766, 1772, 1774, 1783, 1787, 1795, 1800, 1806, 1808, 1810, 1814, 1816, 1822, 1825, 1829, 1841, 1843, 1845, 1852, 1862, 1864, 1866, 1867, 1869, 1873, 1882, 1883, 1885, 1890, 1895, 1901, 1906, 1912, 1915, 1916, 1919, 1920, 1921, 1926, 1931, 1933, 1936, 1938, 1940, 1943, 1945, 1951, 1956, 1957, 1961, 1963, 1965, 1970, 1974, 1979, 1982, 1986, 1989, 1990, 1996, 1998, 2001, 2003, 2005, 2018, 2020, 2021, 2022, 2024, 2025, 2037, 2039, 2041, 2042, 2045, 2046, 2047, 2050, 2052, 2054, 2056, 2062, 2086, 2087, 2088, 2093, 2099, 2102, 2105, 2110, 2113, 2119, 2124, 2126, 2131, 2135, 2137, 2144, 2154, 2157, 2159, 2166, 2167, 2168, 2170, 2172, 2176, 2178, 2179, 2180, 2182, 2184, 2189, 2190, 2191, 2195, 2196, 2202, 2203, 2207, 2213, 2217, 2218, 2223, 2224, 2229, 2232, 2233, 2235, 2242, 2243, 2245, 2249, 2251, 2252, 2255, 2261, 2264, 2265, 2267, 2270, 2274, 2283, 2290, 2291, 2293, 2294, 2298, 2300, 2310, 2313, 2315, 2316, 2323, 2334, 2337, 2342, 2345, 2346, 2349, 2350, 2352, 2359, 2360, 2362, 2366, 2372, 2374, 2379, 2383	33.37B	2.13×10^{-5}	2239.002
E [28]	1, 2, 3, 4, 5, 7, 8, 9, 10, 11, 12, 13, 14, 16, 17, 18, 19, 20, 21, 22, 23, 25, 26, 28, 29, 31, 32, 35	1.87B	4×10^{-5}	111.178

TABLE VII: Analysis of joint optimal PMU placement and data pruning under faults in real power systems

Test syst.	Conventional optimal PMU placement and system-aware data pruning						Joint optimal PMU placement and data pruning					
	BW consumption		Average node estim-ation error $(\times 10^{-3})$		Obs. loss		BW consumption		Average node estim-ation error $(\times 10^{-3})$		Obs. loss	
	SPL	SLL	SPL	SLL	SPL	SLL	SPL	SLL	SPL	SLL	SPL	SLL
A	3.53B	3.29B	0.537	0.521	0.371	0.334	1.17B	1.17B	0.0303	0.0301	0	0
B	6.46B	6.13B	0.411	0.4	0.211	0.402	1.82B	1.82B	0.0175	0.0173	0	0
C	16.21B	15.78B	5.5	5.3	0.383	0.4	4.87B	4.87B	0.0333	0.0331	0	0
D	162.77B	163.51B	1.344	1.245	0.323	0.336	33.37B	33.37B	0.0216	0.0211	0	0
E	5.87B	5.11B	1.078	0.997	0.115	0.123	1.87B	1.87B	0.0402	0.04	0	0

E. Joint Optimal PMU Placement in Actual Power Networks

Tables V and VI present the utilization of the proposed joint optimal PMU placement and data pruning in actual power networks, namely A: new England 39-bus system, B: southern India 72-bus system, C: Iranian 242-bus system, D: Polish 2383-bus system, and E: practical grid of China. From Table V we observe that, with system-aware optimum data pruning in conventional optimal PMU placement framework, average node estimation error as well as aggregate network bandwidth consumption are more than the values obtained in the proposed joint optimal PMU placement and data pruning setup. It is observed from Table VI that the revised optimal PMU placement vector results in a network-level maximum bandwidth saving, with a highly accurate grid estimation.

Further, from Table VII we note that the observability in the proposed strategy is 100%, while there is negligible change in bandwidth consumption and average node estimation error during grid disturbances caused by PMU or line loss. This can be attributed to the redundancy in the proposed PMU placement framework. Therefore, we conclude that the proposed PMU placement strategy leads to significant communication bandwidth saving while providing a reinforced immunity to power system faults or communication specific adversities.

VI. Concluding Remarks

In this paper a novel jointly optimal PMU placement and system-aware data pruning strategy has been proposed for communication resource efficient smart grid monitoring. The proposed joint optimization aimed at reducing the data volume to be transmitted from the smart PMUs to PDC without compromising on the error threshold at all spatial nodes in the smart grid system. SEP has been mathematically modeled, to define the optimal setting for per-attribute tolerance thresholds. It has been noted that there is a trade-off between achieving the optimum PMU deployment considering only grid observability and attaining an efficient communication resource utilization. This offers an alternate viewpoint on the optimal PMU placement formulation. To this end, a weighted grid incidence matrix has been proposed based on node importance factor, thus devising a power-communication mutual optimal formulation. The results have demonstrated that the jointly optimal placement formulation renders a significantly different optimal PMU deployment solution with an overall higher data compressibility, thereby saving communication resources, while maintaining the grid monitoring quality.

Appendix

A. Proof of Lemma 1

Consider, a PMU installed at node i measures h parameters, s.t. $\mathscr{X}_j = \{x_{1,j}, x_{2,j}, \cdots, x_{h,j}\}$, and there are W optimally placed PMUs, s.t. $j = 1, \cdots, W$. Let $f_{j,i,\nu}(\mathscr{X}_j)$ be the map function to get the νth pseudo-measurement for ith pseudo-monitored node, s.t. $\nu = 1, \cdots, h$, and $i = 1, \cdots, M$. Then, the νth pseudo-measurement at node i is $x_{\nu,i} = \sum_{j=1}^{W} f_{j,i,\nu}(\mathscr{X}_j)$. Since the data at the PDC have estimation error, we have $\tilde{x}_{\nu,j} = x_{\nu,j} + \Delta x_{\nu,j}$. For the complete parameter set $\tilde{\mathscr{X}}_j = \mathscr{X}_j + \mathbf{e}_j$, where the estimation error vector $\mathbf{e}_j = [\Delta x_{1,j}, \cdots, \Delta x_{W,j}]^T$, we write $x_{\nu,i} + \Delta x_{\nu,i} = \sum_{j=1}^{W} f_{j,i,\nu}(\mathscr{X}_j + \mathbf{e}_j)$. Using Taylor's expansion,

$$\Delta x_{\nu,i} = \sum_{j=1}^{W} \mathbf{D}^T f_{j,i,\nu}(\mathscr{X}_j)\mathbf{e}_j \tag{A1}$$

where $\mathbf{D} = [\frac{\partial}{\partial x_{1,j}}, \cdots, \frac{\partial}{\partial x_{W,j}}]^T$. Extending (A1) for all nodes, SEP in $x_{\nu,j}$ across M pseudo-monitored nodes is

$$\boldsymbol{\theta}_\nu = \mathbf{A}_{1,\nu}\mathbf{e}_1 + \mathbf{A}_{2,\nu}\mathbf{e}_2 + \cdots + \mathbf{A}_{W,\nu}\mathbf{e}_W \overset{(b)}{=} \mathbf{A}_\nu^T \mathbf{e} \tag{A2}$$

where $\boldsymbol{\theta}_\nu$ is the SEP in the νth pseudo-measurement across M pseudo-monitored nodes, s.t. $\boldsymbol{\theta}_\nu = [\Delta x_{\nu,1}, \Delta x_{\nu,2}, \cdots, \Delta x_{\nu,M}]^T$, and $\mathbf{A}_{j,\nu} = [\mathbf{D}^T f_{j,1,\nu}, \mathbf{D}^T f_{j,2,\nu}, \cdots, \mathbf{D}^T f_{j,M,\nu}]^T$ is the SEP matrix for PMU installed at jth node. (A2) can be concisely represented through equality (b), where $\mathbf{A}_\nu = [\mathbf{A}_{1,\nu}, \mathbf{A}_{2,\nu}, \cdots, \mathbf{A}_{W,\nu}]^T$, and $\mathbf{e} = [\mathbf{e}_1, \mathbf{e}_2, \cdots, \mathbf{e}_W]^T$.

B. Proof of Theorem 1

Using Kirchhoff's voltage law (KVL) on the 6-bus system,

$$\begin{aligned} E_6\angle\delta_6 &= E_5\angle\delta_5 + jX_{65}I_{65}\angle\phi_{65} \\ E_1\angle\delta_1 &= E_4\angle\delta_4 - jX_{41}I_{41}\angle\phi_{41} \\ E_3\angle\delta_3 &= E_4\angle\delta_4 + jX_{34}I_{34}\angle\phi_{34} \\ E_2\angle\delta_2 &= E_5\angle\delta_5 - jX_{52}I_{52}\angle\phi_{52} \end{aligned} \tag{B1}$$

where E_j is the voltage of bus j at phase δ_j, and I_{ij} is the current on link i-j at phase ϕ_{ij}. The reactance between bus i and j is given as X_{ij}, with $X_{ij} = X_{ji}$. Therefore, using Lemma 1 in (B1), the error propagated in the voltage pseudo-measurements is written as

$$\boldsymbol{\Delta}\mathbf{E} = \mathbf{J}_1\boldsymbol{\Delta}\mathbf{E}_P + \mathbf{J}_2\boldsymbol{\Delta}\boldsymbol{\delta}_P + \mathbf{J}_3\boldsymbol{\Delta}\mathbf{I}_P + \mathbf{J}_4\boldsymbol{\Delta}\boldsymbol{\phi}_P \tag{B2}$$

where $\boldsymbol{\Delta}\mathbf{E} = [\Delta E_6, \Delta E_1, \Delta E_3, \Delta E_2]^T$, $\boldsymbol{\Delta}\mathbf{E}_P = [E_5, E_4]^T$, $\boldsymbol{\Delta}\boldsymbol{\delta}_P = [\delta_5, \delta_4]^T$, $\boldsymbol{\Delta}\mathbf{I}_P = [I_{65}, I_{41}]^T$, and $\boldsymbol{\Delta}\boldsymbol{\phi}_P = [\phi_{65}, \phi_{41}]^T$. $\mathbf{J}_k$, $k \in \{1, \cdots, 4\}$ are the respective attribute's error gain matrices of appropriate dimension. Further, let us define $[F_1, \cdots, F_4]^T \overset{(def)}{=} [E_6, E_1, E_3, E_2]^T$. For the 6-bus test system considered here, these matrices are of order 4×2. Therefore, if $\mathbf{J}_k(i,j)$ denotes the (i,j)th entry of the kth $\mathbf{J}$-matrix, then the entries are: $\mathbf{J}_1(k,1) = \frac{\partial F_i}{\partial E_5}$, $\mathbf{J}_1(k,2) = \frac{\partial F_i}{\partial E_4}$, $\mathbf{J}_2(k,1) = \frac{\partial F_i}{\partial \delta_5}$, $\mathbf{J}_2(k,2) = \frac{\partial F_i}{\partial \delta_4}$, $\mathbf{J}_3(k,1) = \frac{\partial F_i}{\partial I_{65}}$, $\mathbf{J}_3(k,2) = \frac{\partial F_i}{\partial I_{41}}$, $\mathbf{J}_4(k,1) = \frac{\partial F_i}{\partial \phi_{65}}$ and, $\mathbf{J}_4(k,2) = \frac{\partial F_i}{\partial \phi_{41}}$.

C. Proof of Theorem 2

Applying Kirchhoff's current law (KCL) and KVL at pseudo-monitored nodes of the IEEE 6-bus network we get

$$\begin{aligned} I_{46}\angle\phi_{46} &= \frac{E_4\angle\delta_4 - E_6\angle\delta_6}{jX_{46}} \\ I_{16}\angle\phi_{16} &= I_{46}\angle\phi_{46} + I_{65}\angle\phi_{65} + I_{L6}\angle\phi_{L6} \\ I_{34}\angle\phi_{34} &= I_{46}\angle\phi_{46} + I_{41}\angle\phi_{41} + I_{L4}\angle\phi_{L4} \\ I_{23}\angle\phi_{23} &= I_{34}\angle\phi_{34} + I_{L3}\angle\phi_{L3} \end{aligned} \tag{C1}$$

where I_{Li} denotes the load current out of ith bus at a phase ϕ_{Li}. Again, using Lemma 1 in (C1), the error propagated in current pseudo-measurements is given as

$$\boldsymbol{\Delta}\mathbf{I} = \mathbf{H}_1\boldsymbol{\Delta}\mathbf{E}_P + \mathbf{H}_2\boldsymbol{\Delta}\boldsymbol{\delta}_P + \mathbf{H}_3\boldsymbol{\Delta}\mathbf{I}_P + \mathbf{H}_4\boldsymbol{\Delta}\boldsymbol{\phi}_P \tag{C2}$$

where $\mathbf{H}_k$, for $k \in \{1, \cdots, 4\}$ are the respective attribute's error gain matrices of appropriate dimension for determining error propagated in current pseudo-measurements. Again, for the standard IEEE 6-bus system, these matrices are of order 4×2. Further, lets define $[G_1, \cdots, G_2]^T \overset{(def)}{=} [I_{46}, I_{16}, I_{34}, I_{23}]^T$. Under the notations defined in Appendix B, the matrix entries can be defined as $\mathbf{H}_1(k,1) = \frac{\partial G_k}{\partial E_5}$, $\mathbf{H}_1(k,2) = \frac{\partial G_k}{\partial E_4}$, $\mathbf{H}_2(k,1) = \frac{\partial G_k}{\partial \delta_5}$, $\mathbf{H}_2(k,2) = \frac{\partial G_k}{\partial \delta_4}$, $\mathbf{H}_3(k,1) = \frac{\partial G_k}{\partial I_{65}}$, $\mathbf{H}_3(k,2) = \frac{\partial G_k}{\partial I_{41}}$, $\mathbf{H}_4(k,1) = \frac{\partial G_k}{\partial \phi_{65}}$ and, $\mathbf{H}_4(k,2) = \frac{\partial G_k}{\partial \phi_{41}}$.

Remark 5. *For tractability, we assume a perfect knowledge of the load data. Thus, an error in its value is not considered.*

However, considering such an error does not impact the analysis presented here. It only adds an extra dimension to the error vector and thus increases the size of $\mathbf{H}_i$, $i \in \{1, \cdots, 4\}$.

D. Proof of Theorem 3

The apparent power in link i-j is given as $S_{ij} = (V_i \angle \delta_i - v_j \angle \delta_j) I_{ij} \angle (-\phi_{ij})$. Thus, the active power P_{ij} is given as $P_{ij} = \Re(S_{ij})$, where $\Re(\cdot)$ denotes the real part. Therefore, using Lemma 1 and the active power computed through (B1) and (C1), the error propagation into the active power pseudo-measurements can be written as

$$\mathbf{\Delta P} = \mathbf{R}_1 \mathbf{\Delta E}_P + \mathbf{R}_2 \mathbf{\Delta \delta}_P + \mathbf{R}_3 \mathbf{\Delta I}_P + \mathbf{R}_4 \mathbf{\Delta \phi}_P \quad \text{(D1)}$$

where $\mathbf{R}_k$, for $k \in \{1, \cdots, 4\}$ denotes 4×2 error gain matrix. For IEEE 6-bus system, the respective error gain matrix entries can be expressed as $\mathbf{R}_1(k,1) = \frac{\partial L_k}{\partial E_5}$, $\mathbf{R}_1(k,2) = \frac{\partial L_k}{\partial E_4}$, $\mathbf{R}_2(k,1) = \frac{\partial L_k}{\partial \delta_5}$, $\mathbf{R}_2(k,2) = \frac{\partial L_k}{\partial \delta_4}$, $\mathbf{R}_3(k,1) = \frac{\partial L_k}{\partial I_{65}}$, $\mathbf{R}_3(k,2) = \frac{\partial L_k}{\partial I_{41}}$, $\mathbf{R}_4(k,1) = \frac{\partial L_k}{\partial \phi_{65}}$ and, $\mathbf{R}_4(k,2) = \frac{\partial L_k}{\partial \phi_{41}}$, where $[L_1, \cdots, L_4]^T \overset{(def)}{=} [P_{46}, P_{16}, P_{34}, P_{23}]^T$.

E. Proof of Theorem 4

For, reactive power we have $Q_{ij} = \Im(S_{ij})$, where $\Im(\cdot)$ denotes the imaginary part. Using Lemma 1 as in the prior proof, the error propagation into the reactive power pseudo-measurements are given as

$$\mathbf{\Delta Q} = \mathbf{T}_1 \mathbf{\Delta E}_P + \mathbf{T}_2 \mathbf{\Delta \delta}_P + \mathbf{T}_3 \mathbf{\Delta I}_P + \mathbf{T}_4 \mathbf{\Delta \phi}_P \quad \text{(E1)}$$

where $\mathbf{T}_k$, for $k \in \{1, \cdots, 4\}$ are the reactive power error gain matrices of appropriate dimensions against the measurement bases as defined. Lets define $[K_1, \cdots, K_4]^T \overset{(def)}{=} [Q_{46}, Q_{16}, Q_{34}, Q_{23}]^T$. Then, for an IEEE 6-bus system, these error gain matrices are defined as $\mathbf{T}_1(k,1) = \frac{\partial K_k}{\partial E_5}$, $\mathbf{T}_1(k,2) = \frac{\partial K_k}{\partial E_4}$, $\mathbf{T}_2(k,1) = \frac{\partial K_k}{\partial \delta_5}$, $\mathbf{T}_2(k,2) = \frac{\partial K_k}{\partial \delta_4}$, $\mathbf{T}_3(k,1) = \frac{\partial K_k}{\partial I_{65}}$, $\mathbf{T}_3(k,2) = \frac{\partial K_k}{\partial I_{41}}$, $\mathbf{T}_4(k,1) = \frac{\partial K_k}{\partial \phi_{65}}$ and, $\mathbf{T}_4(k,2) = \frac{\partial K_k}{\partial \phi_{41}}$.

REFERENCES

[1] A. K. Mandal, A. Malkhandi, S. De, N. Senroy, and S. Mishra, "A multipath model for disturbance propagation in electrical power networks," *IEEE Trans. Circuits Syst. II: Express Briefs*, pp. 1–1, 2022.

[2] Y. Yan, Y. Qian, H. Sharif, and D. Tipper, "A survey on smart grid communication infrastructures: Motivations, requirements and challenges," *IEEE Commun. Surv. Tutor.*, vol. 15, no. 1, pp. 5–20, 2013.

[3] R. Ma, H.-H. Chen, Y.-R. Huang, and W. Meng, "Smart grid communication: Its challenges and opportunities," *IEEE Trans. Smart Grid*, vol. 4, no. 1, pp. 36–46, 2013.

[4] A. Aligholian, A. Shahsavari, E. M. Stewart, E. Cortez, and H. Mohsenian-Rad, "Unsupervised event detection, clustering, and use case exposition in micro-PMU measurements," *IEEE Trans. Smart Grid*, vol. 12, no. 4, pp. 3624–3636, 2021.

[5] A. Shahsavari, M. Farajollahi, E. M. Stewart, E. Cortez, and H. Mohsenian-Rad, "Situational awareness in distribution grid using micro-PMU data: A machine learning approach," *IEEE Trans. Smart Grid*, vol. 10, no. 6, pp. 6167–6177, 2019.

[6] M. Khan, P. M. Ashton, M. Li, G. A. Taylor, I. Pisica, and J. Liu, "Parallel detrended fluctuation analysis for fast event detection on massive PMU data," *IEEE Trans. Smart Grid*, vol. 6, no. 1, pp. 360–368, 2014.

[7] A. Malkhandi, N. Senroy, and S. Mishra, "A dynamic model of impedance for online thevenin's equivalent estimation," *IEEE Trans. Circ. Syst. II: Express Briefs*, vol. 69, no. 1, pp. 194–198, 2022.

[8] A. K. Mandal and S. De, "Analysis of wireless communication over electromagnetic impulse noise channel," *IEEE Trans. Wireless Commun.*, pp. 1–1, 2022.

[9] F. Zhang, L. Cheng, X. Li, Y. Sun, W. Gao, and W. Zhao, "Application of a real-time data compression and adapted protocol technique for WAMS," *IEEE Trans. Power Syst.*, vol. 30, no. 2, pp. 653–662, 2015.

[10] D. Chu, A. Deshpande, J. M. Hellerstein, and Wei Hong, "Approximate data collection in sensor networks using probabilistic models," in *Proc. 22nd Int. Conf. Data Eng.*, 2006.

[11] S. Santoso, E. J. Powers, and W. M. Grady, "Power quality disturbance data compression using wavelet transform methods," *IEEE Trans. Power Deliv.*, vol. 12, no. 3, 1997.

[12] J. Ning, J. Wang, W. Gao, and C. Liu, "A wavelet-based data compression technique for smart grid," *IEEE Trans. Smart Grid*, vol. 2, no. 1, 2011.

[13] R. Pourramezan, R. Hassani, H. Karimi, M. Paolone, and J. Mahseredjian, "A real-time synchrophasor data compression method using singular value decomposition," *IEEE Trans. Smart Grid*, vol. 13, no. 1, pp. 564–575, 2021.

[14] M. R. Chowdhury, S. Tripathi, and S. De, "Adaptive multivariate data compression in smart metering internet of things," *IEEE Trans. Ind. Informat.*, vol. 17, no. 2, 2021.

[15] P. H. Gadde, M. Biswal, S. Brahma, and H. Cao, "Efficient compression of PMU data in wams," *IEEE Trans. Smart Grid*, vol. 7, no. 5, 2016.

[16] C. A. Jensen, M. A. El-Sharkawi, and R. J. Marks, "Power system security assessment using neural networks: feature selection using fisher discrimination," *" IEEE Power Eng. Rev.*, vol. 16, no. 4, 2001.

[17] S. Tripathi and S. De, "Dynamic prediction of powerline frequency for wide area monitoring and control," *IEEE Trans. Ind. Informat.*, vol. 14, no. 7, 2018.

[18] M. Kamal, M. Farajollahi, H. Nazaripouya, and H. Mohsenian-Rad, "Cyberattacks against event-based analysis in micro-PMUs: Attack models and counter measures," *IEEE Trans. Smart Grid*, vol. 12, no. 2, pp. 1577–1588, 2020.

[19] *Guide for Installation of Multi-Function Phasor Measurement Units (MF-PMUs)*, North American SynchroPhasor Initiative (NASPI), Performance & Standards Task Team (PSTT), 2014. [Online]. Available: https://www.naspi.org/sites/default/files/reference_documents/NASPI_Guide_for_Multifunction_PMUs_tac_20141010.pdf

[20] *Reliability Guideline: PMU Placement and Installation*, North American Electric Reliability Corporation, 2016. [Online]. Available: https://www.nerc.com/comm/RSTC_Reliability_Guidelines/Reliability\%20Guideline\%20-\%20PMU\%20Placement.pdf

[21] F. Aminifar, M. Fotuhi-Firuzabad, and A. Safdarian, "Optimal PMU placement based on probabilistic cost/benefit analysis," *IEEE Trans. Power Syst.*, vol. 28, no. 1, pp. 566–567, 2013.

[22] S. Almasabi and J. Mitra, "Multistage optimal PMU placement considering substation infrastructure," *IEEE Trans. Ind. Appl.*, vol. 54, no. 6, pp. 6519–6528, 2018.

[23] B. Cao, Y. Yan, Y. Wang, X. Liu, J. C.-W. Lin, A. K. Sangaiah, and Z. Lv, "A multiobjective intelligent decision-making method for multistage placement of PMU in power grid enterprises," *IEEE Trans. Ind. Informat.*, pp. 1–9, 2022.

[24] M. Elimam, Y. J. Isbeih, M. S. E. Moursi, K. Elbassioni, and K. H. A. Hosani, "Novel optimal PMU placement approach based on the network parameters for enhanced system observability and wide area damping control capability," *IEEE Trans. Power Syst.*, vol. 36, no. 6, pp. 5345–5358, 2021.

[25] A. A. Saleh, A. S. Adail, and A. A. Wadoud, "Optimal phasor measurement units placement for full observability of power system using improved particle swarm optimisation," *IET Gener. Transm. Distrib.*, vol. 11, no. 7, pp. 1794–1800, 2017.

[26] W. Li, D. Deka, M. Chertkov, and M. Wang, "Real-time faulted line localization and PMU placement in power systems through convolutional neural networks," *IEEE Trans. Power Syst.*, vol. 34, no. 6, pp. 4640–4651, 2019.

[27] C. Rakpenthai, S. Premrudeepreechacharn, S. Uatrongjit, and N. R. Watson, "An optimal PMU placement method against measurement loss and branch outage," *IEEE Trans. Power Deliv.*, vol. 22, no. 1, pp. 101–107, 2007.

[28] M. Esmaili, K. Gharani, and H. A. Shayanfar, "Redundant observability PMU placement in the presence of flow measurements considering contingencies," *IEEE Trans. Power Syst.*, vol. 28, no. 4, pp. 3765–3773, 2013.

[29] S. Kumar, B. Tyagi, V. Kumar, and S. Chohan, "Optimization of phasor measurement units placement under contingency using reliability of

network components," *IEEE Trans. Instrum. Meas.*, vol. 69, no. 12, pp. 9893–9906, 2020.

[30] N. M. Manousakis and G. N. Korres, "Optimal allocation of phasor measurement units considering various contingencies and measurement redundancy," *IEEE Trans. Instrum. Meas.*, vol. 69, no. 6, pp. 3403–3411, 2019.

[31] A. Paul, I. Kamwa, and G. Jóos, "Centralized dynamic state estimation using a federation of extended Kalman filters with intermittent pmu data from generator terminals," *IEEE Trans. Power Syst.*, vol. 33, no. 6, pp. 6109–6119, 2018.

[32] N. Zhou, D. Meng, Z. Huang, and G. Welch, "Dynamic state estimation of a synchronous machine using PMU data: A comparative study," *IEEE Trans. Smart Grid*, vol. 6, no. 1, pp. 450–460, 2015.

[33] S. S. Mousavi-Seyedi, F. Aminifar, and S. Afsharnia, "Parameter estimation of multiterminal transmission lines using joint PMU and SCADA data," *IEEE Trans. Power Deliv.*, vol. 30, no. 3, pp. 1077–1085, 2015.

[34] A. Gorbunov, A. Dymarsky, and J. Bialek, "Estimation of parameters of a dynamic generator model from modal PMU measurements," *IEEE Trans. Power Syst.*, vol. 35, no. 1, pp. 53–62, 2020.

[35] M. Picallo, A. Anta, and B. de Schutter, "Comparison of bounds for optimal PMU placement for state estimation in distribution grids," *IEEE Trans. Power Syst.*, vol. 34, no. 6, pp. 4837–4846, 2019.

[36] T. Baldwin, L. Mili, M. Boisen, and R. Adapa, "Power system observability with minimal phasor measurement placement," *IEEE Trans. Power Syst.*, vol. 8, no. 2, pp. 707–715, 1993.

[37] Q. Li, R. Negi, and M. D. Ilić, "Phasor measurement units placement for power system state estimation: A greedy approach," in *Proc. IEEE PES General Meeting*, 2011, pp. 1–8.

[38] M. Zhou, V. Centeno, J. Thorp, and A. Phadke, "An alternative for including phasor measurements in state estimators," *IEEE Trans. Power Syst.*, vol. 21, no. 4, pp. 1930–1937, 2006.

[39] J. Liu, J. Tang, F. Ponci, A. Monti, C. Muscas, and P. A. Pegoraro, "Trade-offs in PMU deployment for state estimation in active distribution grids," *IEEE Trans. Smart Grid*, vol. 3, no. 2, pp. 915–924, 2012.

[40] R. Gupta, V. Gupta, A. K. Mandal, and S. De, "Learning-based multivariate real-time data pruning for smart PMU communication," in *Proc. IEEE Consum. Commun. Netw. Conf.* IEEE, 2022, pp. 326–331.

[41] M. Awad and R. Khanna, "Support vector regression," *Efficient learning machines: Theories, concepts, and applications for engineers and system designers*, pp. 67–80, 2015.

[42] S. Boyd and L. Vandenberghe, *Convex optimization*. Cambridge university press, 2004.